Contrasting origins of serpentinites in a subduction complex, northern Dominican Republic

Benoit-Michel Saumur[1], Kéiko H. Hattori[1], and Stéphane Guillot[2]
[1]*Department of Earth Sciences, University of Ottawa, 140 Louis Pasteur, Ottawa, Ontario, K1N 6N5, Canada*
[2]*Institut National des Sciences de l'Univers—Centre National de la Recherche Scientifique, University of Grenoble, 1381 rue de la Piscine, 38041 Grenoble, cedex 9, France*

ABSTRACT

Serpentinites in a Tertiary subduction complex in the northern Dominican Republic contain low concentrations of incompatible elements in bulk-rock compositions and high Mg in relict silicate minerals. The forsterite component in olivine ranges from 89.0% to 90.8%, and the enstatite component in orthopyroxene ranges from 89.4% to 91.1%, suggesting that they are mantle peridotites. Two different protoliths are identified for the serpentinites based on the bulk-rock compositions and spinel chemistry: abyssal peridotites and forearc mantle peridotites. Hydrated abyssal peridotites are voluminous and occur in ophiolite complexes in the northern terranes (Puerto Plata Complex and the northern part of the Rio San Juan Complex) and in serpentinite mélanges in the central part of the Rio San Juan Complex. The serpentinite mélanges contain fragments of high-pressure–low-temperature rocks and are interpreted to be tectonic mélanges, representing part of a serpentinite subduction channel. The serpentinites show moderate Al/Si weight ratios (0.026–0.081) in bulk rocks and moderate Cr# (atomic ratio of Cr/[Cr + Al] = 0.20–0.55) in spinel.

Hydrated forearc mantle peridotites occur along major strike-slip faults: the Camú fault zone, and the Septentrional fault zone. They show low bulk-rock Al/Si weight ratios (up to 0.021), high concentration in Ir-group platinum group elements (13.1–24.6 ppb total), and high Cr# (0.48–0.67) in spinel. Raman spectroscopy and X-ray powder diffraction indicate that lizardite is the predominant serpentine species. The absence of antigorite suggests that these serpentinites were derived from a shallow depth (<<35 km) in the mantle wedge. Their occurrence along the major strike-slip fault zones suggests that the faults allowed these serpentinites to protrude from the forearc mantle wedge during oblique transpressive collision of the Caribbean plate with the Bahamas Platform.

INTRODUCTION

Recent studies highlight the importance of serpentinites in subduction zones. Serpentinites can contain up to 13 wt% H_2O and may be stable at depths to 130 km (Wunder and Schreyer, 1997), making them an important host of water and fluid-mobile elements in the mantle (Hattori and Guillot, 2003, 2007). The release of such water during the dehydration of serpentinites may trigger partial melting in the interior of mantle wedges (Hattori and Guillot, 2003). Therefore, serpentinites play a significant role in recycling of elements in subduction zones (Hattori and Guillot, 2007). Furthermore, the volume change associated with this dehydration may be responsible for deep seismic activity in subduction zones (Dobson et al., 2002).

The origin of serpentinites in subduction complexes has been discussed extensively (e.g., Guillot et al., 2000; Ernst, 2004; Hattori and Guillot, 2007). There are three possible protoliths: (1) forearc mantle peridotites hydrated at the base of the mantle wedge by fluids released from subducted slabs, including sediments, (2) abyssal peridotites hydrated at shallow depths near oceanic ridges and the seafloor, and (3) hydrated ultramafic cumulates (e.g., Hattori and Guillot, 2007). An understanding of the origin of serpentinites is important in evaluating the geodynamic evolution of subduction zones and the possible role of serpentinites in the recycling of elements and the global mass balance.

Serpentinites are abundant in the northern Dominican Republic on Hispaniola (Fig. 1), where they belong to one of the largest exposed subduction complexes in the world. This paper presents the distribution, mineralogy, and the compositions of serpentinites in this accretionary complex, and we discuss their origins and the implications for syn- and post-subduction processes.

GEOLOGICAL SETTING

Hispaniola is located on the northern margin of the Caribbean plate (Fig. 1). Until the mid-Cretaceous, it had a location west of its current position, above the NE-dipping Farallon oceanic plate in the Pacific Ocean (Pindell et al., 2005). A major change in the geometry of the plates in the area took place in the mid-Cretaceous. This change involved migration of the arc from the Pacific to the Atlantic Ocean side, reversal of subduction polarity, and the divergence between North and South America, which was partly accommodated by rifting at the proto–Caribbean Ridge (Meschede and Frisch, 1998; Pindell et al., 1988). The proto-Caribbean oceanic lithosphere produced at the ridge subducted beneath the NE-migrating Caribbean plate between the Late Cretaceous and the middle Eocene, until oblique collision of the Caribbean plate with the Bahamas Platform occurred (Goncalves et al., 2000). This produced left-lateral strike-slip faults in northern Hispaniola: the Septentrional fault zone and the Camú fault zone (Mann et al., 1984; Goncalves et al., 2000; Fig. 2A). The Septentrional fault zone is still actively creating displacement along the fault with seismic activity (e.g., Calais et al., 1998).

The northern Dominican Republic (NE margin of Hispaniola; Fig. 1) is mostly covered by sedimentary rocks ranging in age from Miocene to Quaternary (Draper and Nagle, 1991). Only five inliers expose rocks older than middle Eocene (Fig. 1), and these rocks are mostly subduction-related igneous rocks with minor limestones in basins formed during the collision with the Bahamas Platform. The area is in the 1000-km-long Northern serpentinite mélange, which extends from Cuba to Hispaniola (Fig. 1; Lewis et al., 2006). In Cuba, serpentinites are intercalated with fossiliferous mudstones in several locations, and some serpentinite outcrops are interpreted as mudflow and sedimentary breccia deposits (Lockwood, 1971). In northern Dominican Republic, the occurrences of serpentinite blocks are reported in sedimentary

†E-mail: khattori@uottawa.ca

GSA Bulletin; doi: 10.1130/B26530.1; 10 figures; 4 tables; Data Repository item 2009134.

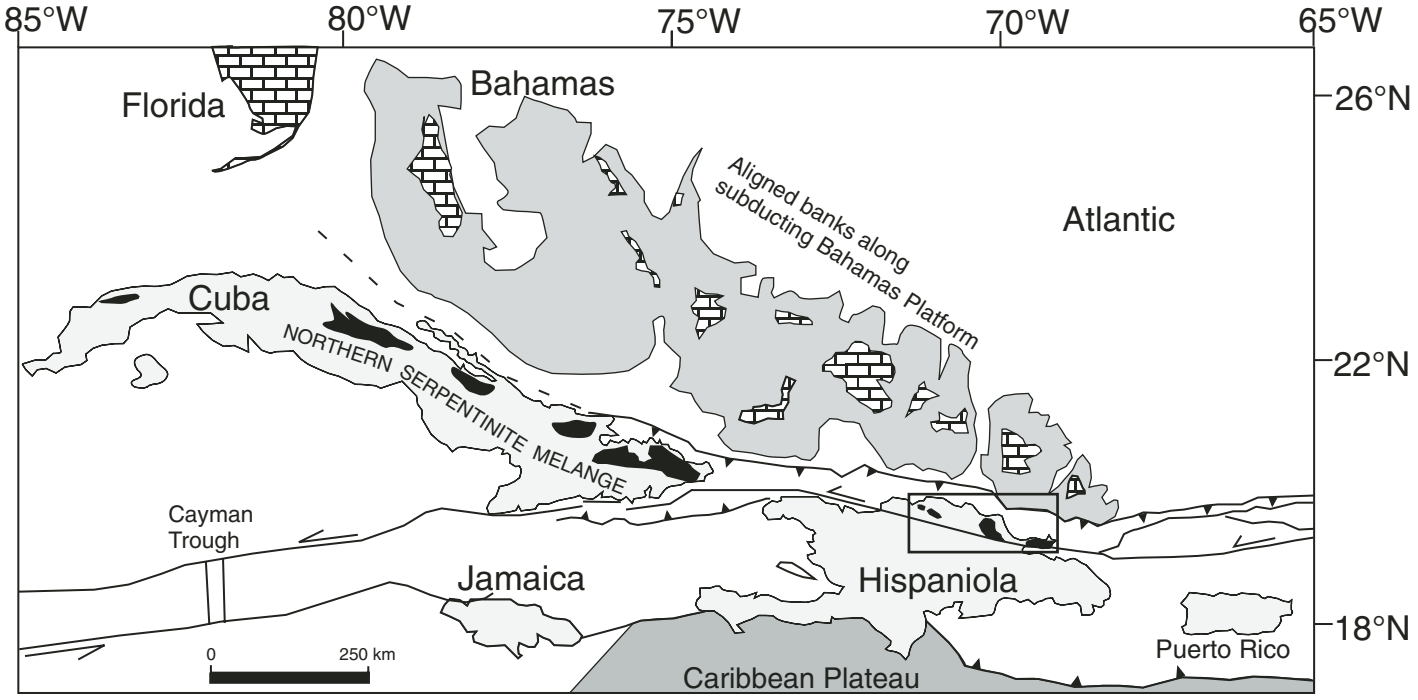

Figure 1. Map of the Greater Antilles and the northeastern Caribbean plate margin (modified from Dolan et al., 1998). The box indicates the study area (see Fig. 2).

olistostrome (Nagle, 1966, cited in Lockwood, 1971), but serpentinites with fossils have not been found. Therefore, we conclude that sedimentary processes were not involved in the emplacement of these serpentinites in the study area in the Dominican Republic.

The study area contains three inliers (Fig. 2A), the Puerto Plata Complex, the Rio San Juan Complex, and the Pedro Garcia Complex. The Puerto Plata Complex consists of the Late Cretaceous to middle Eocene mafic-ultramafic igneous rocks and Paleocene–Eocene volcano-sedimentary units. The mafic-ultramafic igneous rocks consist of variably brecciated and sheared serpentinite, tectonized peridotites, gabbro, and mafic volcanic rocks; they are interpreted as an ophiolitic complex (Pindell and Draper, 1991). Sheeted diabasic dikes were not observed, but brecciated serpentinites commonly contain clasts of altered gabbro and gabbro dikes. The volcano-sedimentary unit contains crystal tuffs and sandy to pebbly turbiditic sedimentary rocks (Fig. 2C). Immature rocks contain clasts of limestone, serpentinites, and volcanic rocks. The Pedro Garcia Complex consists of arc igneous rocks, including tuffs, amygdaloidal mafic lava flows, and dikes with small felsic stocks (Lewis et al., 1990; Draper and Nagle, 1991). A preliminary whole-rock K-Ar age of 72 ± 7 Ma for a mafic flow was reported by Bowin and Nagle, 1982, cited in Lewis et al. (1990).

The Rio San Juan Complex is composed of three parts (Fig. 2B): the Gaspar Hernandez serpentinites in the north, retrograded blueschists and eclogites in the central part, and the Cuaba Gneiss and the Rio Boba Gabbro to the south. The Gaspar Hernandez serpentinites are very similar to serpentinites in the Puerto Plata Complex in texture, mineralogy, and chemical composition. Therefore, these two serpentinites are referred to here as serpentinites from the "northern terranes" (Table 1). The central part of the Rio San Juan Complex is distinguished from the northern terranes because it is essentially composed of high-pressure metamorphic rocks. These rocks are intruded by two serpentinite mélanges, the Jagua Clara mélange and Arroyo Sabana mélange (Fig. 2B); the two mélanges are very similar in appearance, texture, and mineralogy, and they are grouped here as the "serpentinite mélanges." They are matrix-supported tectonic mélanges containing meter-scale blocks of blueschists, eclogites, and metamorphosed felsic rocks aligned to a subvertical foliation. The southern part of the Rio San Juan Complex is composed of the Cuaba Gneiss, which is intruded by the Rio Boba Gabbro (Fig. 2B). The Cuaba Gneiss is made up of oceanic gabbros metamorphosed under amphibolite facies conditions (Abbott et al., 2006). The Cuaba Gneiss contains retrograded eclogites, and lenses (100–500 m long) of serpentinites. Foliation wrapping around these lenses suggests that the serpentinites were emplaced during ductile deformation of the Cuaba Gneiss. Furthermore, large (up to 2 m) serpentinite boulders occur together with boulders of garnet peridotite and eclogite in the narrow (<6 m) and shallow (<30 cm) stream of Rio Cuevas. These serpentinite boulders only occur along the stream, and their large size and angular surface suggest that they come from proximal sources, although outcrops of serpentinite were not identified due to dense vegetation and thick soil. Massive serpentinites occur near the intersection of the Septentrional fault zone and Bajabonico fault in the southern part of the Rio San Juan Complex (Figs. 2A and 2B).

The three groups of serpentinites in the study area are thus the northern terranes, tectonic mélanges, and exposures along major strike-slip faults (Table 1). The second occurrence, mélange-related serpentinites, is clearly distinguished in the field from the other occurrences because it contains tectonic fragments in the matrix of serpentinites, whereas the other two are massive in outcrops. Furthermore, all hand specimens of serpentinites are similar in appearance, with no clue as to their origin. Fault-related serpentinites do not show foliations or fault-related fabrics. Therefore, classification relied on geochemical data after considering sample distribution.

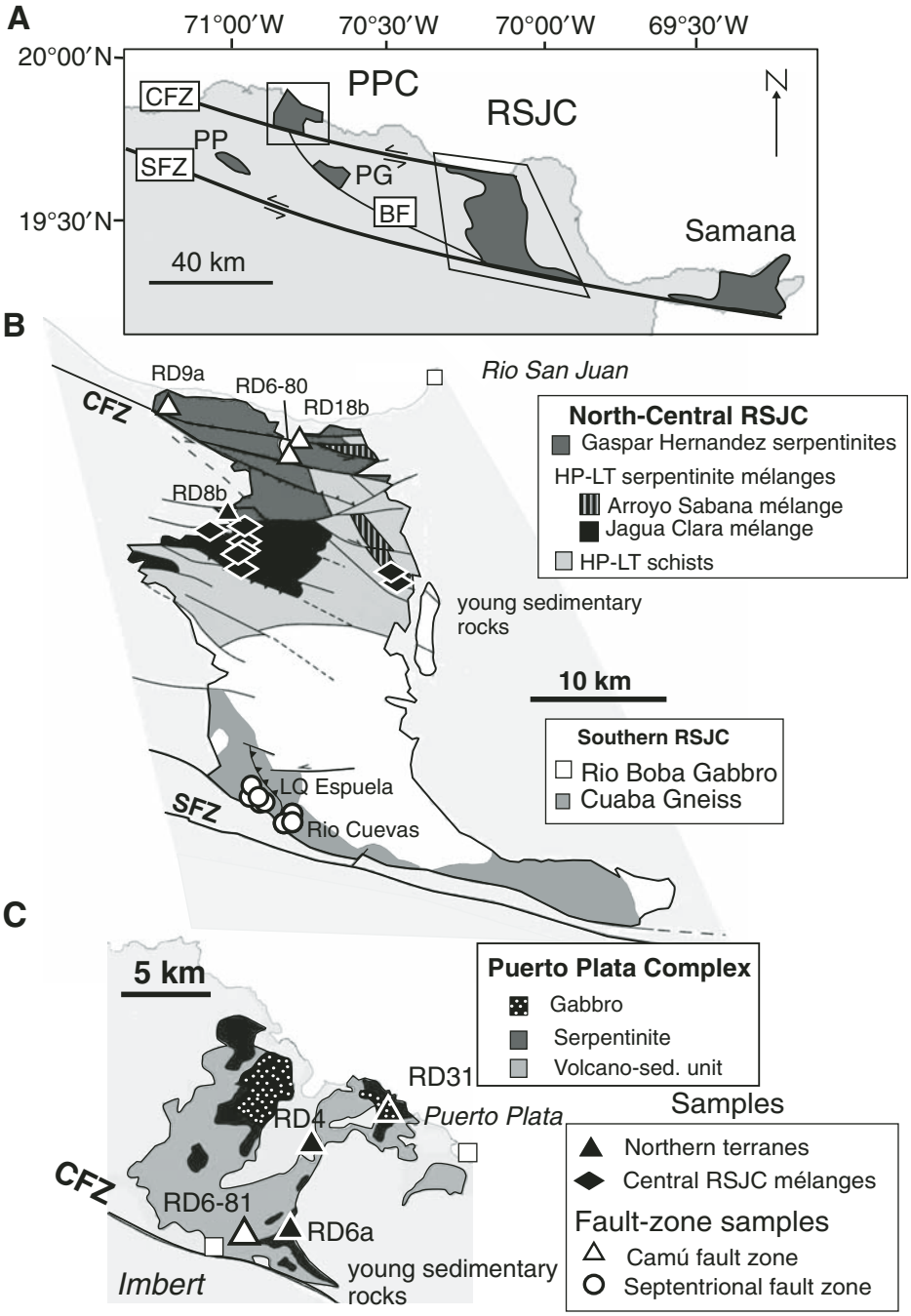

Figure 2. The locations of major strike-slip faults and inliers (dark areas) in the northern Dominican Republic. Most strike-slip motion in the area has been concentrated along the Septentrional (SFZ) and Camú (CFZ) fault zones. Inliers expose pre–mid-Eocene subduction-related rocks (modified from Draper and Nagle, 1991), and the rest of the area is covered by late Eocene, Neogene, and Quaternary sedimentary rocks. BF—Bajabonico fault, CFZ—Camú fault zone, PG—Pedro Garcia Complex, PP—Palma Picada Complex, PPC—Puerto Plata Complex, RSJC—Rio San Juan Complex. (B) Simplified geology of the Rio San Juan Complex and (C) the Puerto Plata Complex, with locations of samples. Open triangles represent samples along the Camú fault zone; filled triangles represent samples in the northern terranes (Puerto Plata Complex and the Gaspar Hernandez serpentinites). Dark flat diamonds indicate serpentinites from tectonic mélanges (Arroyo Sabana mélange, Jagua Clara Mélange). Open circles represent serpentinites adjacent to the Septentrional fault zone near Lomá Quita Espuela (5 samples) and Rio Cuevas (3 samples). Symbols are consistent throughout this paper. Other units shown in the map are the late Rio Boba Gabbro intrusion and the Cuaba Gneiss. Map was modified from Mann et al. (1991); Lewis et al. (1990); Pindell and Draper (1991); Draper and Nagle (1991); and Abbott et al. (2006). Note that Arroyo Sabana mélange occurs in two places, including a small wedge-shaped area in the northern terranes. Sampling locations in UTM coordinates are given in the GSA Data Repository (see text footnote 1). HP-LT—high-pressure–low-temperature.

Sampling

Serpentinite samples were collected in the northern terranes (Table 1) in the Puerto Plata Complex (RD31, RD4, RD6a) and the Gaspar Hernandez serpentinites of the northern Rio San Juan Complex (RD8b) (Fig. 2). Samples from the tectonic mélanges in the central Rio San Juan Complex include two from the Arroyo Sabana mélange (RD87, RD89) and six from the Jagua Clara mélange (RD21a, RD91, RD94, RD6–50c, RD6–52a, RD6–54a) (Fig. 2). Samples of mélange serpentinites (Table 1) are matrix serpentinite free from fragments of blueschists and eclogites. In the southern part of the Rio San Juan Complex, near the Septentrional fault zone, five serpentinite samples were collected from large (~100 m) outcrops (RD34a, RD34c, RD68, RD6–36a, RD6–36c) in Lomá Quita Espuela. Three serpentinite boulders (>3 m in size) were sampled in the stream of Rio Cuevas (RD45, RD48, RD60) near the Septentrional fault zone (Fig. 2B). Samples of serpentinites from fault zones (Table 1) were also collected along the Camú fault zone (RD9A, RD18b, RD6–80, RD6–81) (Fig. 2B). The outcrops and their locations are described in the GSA Data Repository.[1]

[1]GSA Data Repository item 2009134, 1. description of outcrops and description of samples, is available at http://www.geosociety.org/pubs/ft2009.htm or by request to editing@geosociety.org.

ANALYTICAL PROCEDURE

Mineral compositions were determined using a CAMEBAX MBX electron probe in the wavelength dispersive method. Counting times were 15 s per element, except for Fe (20 s) and Ni (40 s). A 15 kV accelerating voltage and a 20 nA beam current were applied. The calibration used wollastonite (Si, Ca), synthetic spinel (Al), synthetic Cr_2O_3 (Cr), forsterite (Mg), synthetic $MnTiO_3$ (Mn, Ti), vanadium metal (V), albite (Na), fayalite (Fe in silicates), and synthetic Fe_2O_2 (Fe in oxides). Fe^{3+} contents of spinel were calculated assuming a stoichiometric composition.

Major- and minor-element concentrations were determined using a Philips PW 2400 X-ray fluorescent spectrometer at the University of Ottawa after fusing bulk-rock powder with a flux composed of 78.5% $Li_2B_4O_7$ and 21.5% $LiBO_2$. Sulfur and Cu were determined using a VISTA-PRO inductively coupled plasma–atomic emission spectrometer (ICP-AES) after digesting samples in aqua regia. Lead concentrations were determined by HP 4500 inductively coupled plasma–mass spectrometer at the University of Ottawa after digestion of samples with a HF-HNO_3 mixture. Platinum group element (PGE) concentrations were determined by an isotopic-dilution technique using a mixed spike of ^{101}Ru, ^{105}Pd, ^{190}Os, ^{191}Ir, and ^{194}Pt. The analytical procedure is essentially the same as that described by Guillot et al. (2000) and Hattori and Guillot (2007). PGEs were preconcentrated in a Ni-sulfide bead that was dissolved in 6 N HCl, and the filtrate was dissolved in concentrated HNO_3 before analysis with HP 4500 at the University of Ottawa. Blanks were 0.002–0.007 ng Ir/g flux, 0.002–0.006 ng Os/g flux, 0.07–16 ng Pt/g flux, 0.03–0.9 ng Pd/g flux, and 0.002–0.007 ng Ru/g flux. These values are negligible compared to amounts in the samples, and thus blank corrections were not applied to the results.

Serpentine minerals were identified using a micro-Raman spectrometer equipped with a Nd-YAG laser at a wavelength of 532 nm, which was focused to ~10 µm diameter on the specimen surface. A Phillips X'PERT X-ray diffractometer was also used to verify the mineralogy of bulk samples.

PETROLOGY OF SERPENTINITES

Serpentine Mineralogy and Mineral Assemblages

Serpentinites from the northern terranes and fault zones were completely hydrated, with high loss on ignition (LOI; ~13 wt%; Table 2), and they were composed of fine-grained lizardite and minor disseminated magnetite. Lizardite was pseudomorphic, retaining the shape of original olivine grains and showing hourglass texture. No antigorite was detected in Raman spectra and X-ray powder diffraction patterns (Figs. 3 and 4). Several fault-zone samples from Lomá Quita Espuela contained fine-grained talc, blades of tremolite, and rare cummingtonite. Although the metamorphic grade was mostly greenschist facies, the mineral assemblage suggests that an amphibolite facies condition was attained locally (e.g., Evans, 1977). Lizardite is known to be metastable under low amphibolite facies condition (Dungan, 1977).

Samples from the tectonic mélanges were also totally hydrated (~11% LOI; Table 2) and were composed of blades of antigorite and fine-grained magnetite (Fig. 3B). Antigorite blades were penetrative, overprinting the original textures of rocks and minerals. Rare pseudomorphic lizardite replacing olivine with hourglass texture occurred in mélange sample RD94, but such pseudomorphic lizardite was for the most part overprinted by penetrative blades of antigorite. The occurrence of chlorite, talc, tremolite (Fig. 4), and antigorite in several samples suggests blueschist to amphibolite facies conditions (e.g., Evans, 1977).

Chromian Spinel

Cr-spinel grains (1–3 mm) were mostly subhedral to anhedral and were rimmed by magnetite and a mixture of magnetite and chlorite. The cores of spinel grains are interpreted to be primary, as they have similar compositions in individual samples (Table 3; Fig. 5). The cores of spinel grains from the northern terrane serpentinites plot in the field of abyssal peridotites (Fig. 5A; Table 3). The northern terrane samples RD4 and RD6a have low Cr# (= atomic ratio of Cr/[Cr + Al]; 0.20–0.40), whereas northern terrane samples RD31 and RD8b have moderate Cr# (~0.53) and higher YFe^{3+} (= atomic ratio of $Fe^{3+}/[Fe^{3+} + Cr + Al]$; 0.04–0.11), similar to abyssal plagioclase peridotite (Fig. 5B).

The cores of spinel in fault-zone serpentinites along the Camú fault zone have moderately high Cr# (0.47–0.69) and XMg (= atomic ratio of $Mg/[Mg + Fe^{2+}]$), between 0.62 and 0.50, and they generally plot within the field of forearc mantle peridotites (Table 3; Fig. 5). Furthermore, they have low YFe^{3+} contents (<0.04; Table 3; Fig. 5B).

The cores of spinel grains in fault-zone serpentinites (RD34c, RD68, RD45, RD48, RD6–36a) along the Septentrional fault zone contain low TiO_2 (<0.21 wt%), low YFe^{3+} (0.03–0.10), and moderate Cr# (0.48–0.67). The compositions are similar to those from the Camú fault zone, but they have low XMg (0.50–0.40) compared to Camú fault zone spinel. Therefore, the spinel grains from fault-zone serpentinites show two different trends in the XMg versus Cr# diagram (Fig. 5A). Furthermore, the values of YFe^{3+} in Septentrional fault zone spinels are slightly higher than those from the Camú fault zone.

Cr-spinel grains in serpentinites from tectonic mélanges are all altered to ferritchromite or aggregates of fine-grained, Cr-bearing magnetite. Spinel grains in mélange samples RD89 and RD94 contain relict Cr-spinel (<0.1 mm), but compositions vary greatly from one grain to another in one thin section, indicating that they have been altered. Therefore, these compositions are not listed in this paper.

Olivine and Orthopyroxene

Olivine is commonly replaced by pseudomorphic lizardite showing hourglass textures and containing dissemination of fine-grained dusty magnetite. Primary olivine is only preserved in fault-zone sample RD68 and mélange samples RD6–52a and RD94. Olivine from fault-zone sample RD68 is slightly higher in Mg ($Fo_{90.8}$) than olivine in mélange samples ($Fo_{89–90.1}$) (Table 4). Orthopyroxene (1–2 mm) is replaced by pseudomorphic lizardite bastites. Primary orthopyroxene is found in only four samples (fault-zone samples RD18b, RD68, RD34, and mélange sample RD94). All have similar compositions characterized by high Mg ($En_{89.4–91.1}$) and low Al_2O_3 (<2.23 wt%; Table 4).

BULK-ROCK COMPOSITIONS

Major Elements

All samples from the study area have refractory bulk-rock compositions with low contents of immobile incompatible elements, such as Al, Ti, and V (Table 2; Fig. 6). Most samples are high in immobile refractory elements, such as Ni (>2000 ppm) and Cr (>2200 ppm). Bulk-rock Mg# (= atomic ratio of $Mg*100/[Mg + Fe_{total}]$) is high, ranging between 88.0 and 91.0, and CaO is low (less than 1 wt%) for most samples. Calcium is known to be mobile during seafloor hydrothermal activity because clinopyroxene is susceptible to alteration by saline fluids (Allen and Seyfried, 2003). However, low CaO content is likely a primary feature because the data are consistent with low Al_2O_3 and high Mg# and Cr contents. The bulk-rock compositions suggest that most samples were initially dunites or harzburgites. Mélange samples RD6–52a and RD6–54a are exceptions; they have high Ca (~3.0 wt%) and low bulk Mg# (86.7–87.2), suggesting that they were originally lherzolite. These samples still contain relatively low Al (<1.34 wt%) and high

TABLE 1. SUMMARY OF THE OCCURRENCES AND SELECTED CHARACTERISTICS OF SERPENTINITES IN THE NORTHERN DOMINICAN REPUBLIC

	Location	Samples*	Serpentine†	Relict primary minerals§	Bulk rock Al/Si weight ratio	Bulk rock ∑IPGE (ppb)#	Origin
Northern terranes	Puerto Plata Complex	4, 6a, 31	Lizardite	Sp (Cr# 0.20–0.55, XMg 0.53–0.70)	0.025–0.056	12.8–16.4	Abyssal peridotite
	Gaspar Hernandez	8b	Lizardite	Sp (Cr# 0.52, XMg 0.54)	0.046	13.7	Abyssal peridotite
Mélanges in central Rio San Juan Complex	Arroyo Sabana	87, 89	Antigorite		0.072–0.081	10.8–11.7	Abyssal peridotite
	Jagua Clara	21a, 91, 94, 6-50c, 6-52a, 6-54a	Antigorite lizardite	Ol ($Fo_{89–90.1}$) Opx ($En_{89.6–90.5}$)	0.031–0.071	8.9–14.4	Abyssal peridotite
Fault zones	Camú fault zone	9a,18b, 6-80, 6-81	Lizardite	Sp (Cr# 0.47–0.69, XMg 0.50–0.62) Opx ($En_{90.1}$)	0.012–0.021	14.5–26.6	Mantle wedge
	Septentrional fault zone	L.Q. Esp.: 34a, 34c, 68, 6-36a, 6-36c Rio Cuevas: 45, 48, 60	Lizardite	Sp (Cr# 0.48–0.66, XMg 0.40–0.50) Ol ($Fo_{90.8}$) Opx ($En_{89.4–91.1}$)	0.017–0.020	13.1–24.6	Mantle wedge

*Prefix of RD is omitted.

†The phases of individual serpentinite grains were identified at the University of Ottawa using a micro-Raman spectrometer equipped with a frequency doubled Nd-YAG laser at a wavelength of 532 nm. The laser beam was focused ~10 µm in diameter on samples. Our methodology is similar to that described by Groppo et al. (2006). The mineralogy of bulk samples was examined using an X-ray powder diffractometer (Phillips X'PERT X-ray diffractometer) at the University of Ottawa.

§Abbreviations: Ol—olivine, Sp—spinel, Opx—orthopyroxene, Cr#—atomic ratio of Cr/(Cr + Al) in spinel, XMg—atomic ratio of Mg/(Mg + Fe^{2+}).

#IPGE: Ir-group platinum group elements (PGEs; Os, Ir, Ru).

TABLE 2. BULK-ROCK COMPOSITION OF SERPENTINITES FROM THE NORTHERN DOMINICAN REPUBLIC

		Northern terranes				Camú fault zone				Mélange								SFZ–Rio Cuevas			SFZ–Loma Quita Espuela				
		RD4	RD6a	RD8b	RD31	RD9a	RD18b	RD6-80	RD6-81	RD87	RD89	RD91	RD94	RD6-50c	RD6-52a	RD21a	RD6-54a	RD48	RD60	RD45	RD34a	RD34c	RD68	RD6-36a	RD6-36c
SiO_2	%	39.9	39.3	39.3	40.5	41.1	39.7	41.1	40.7	41.9	42.2	42.08	44.72	42.2	42.3	38.8	36.0	40.8	40.8	39.6	41.3	39.8	42.3	40.8	41.6
TiO_2	%	0.04	0.02	0.02	0.02	0.02	0.02	0.02	0.02	0.06	0.11	0.07	0.05	0.02	0.11	0.03	0.04	0.02	0.02	0.02	0.03	0.02	0.02	0.02	0.02
Al_2O_3	%	1.99	0.9	1.6	1.44	0.53	0.69	0.36	0.61	3.01	2.69	2.23	2.51	2.63	1.16	1.24	1.36	0.44	0.76	0.4	0.61	0.7	0.74	0.69	0.71
Fe_2O_3*	%	9.34	7.83	10.03	8.19	9.11	8.52	9.23	8.36	9.37	7.78	7.94	8.14	8.47	9.89	11.21	10.71	7.98	7.72	8.26	9.76	8.75	9.19	8.60	8.84
MnO	%	0.07	0.10	0.06	0.06	0.09	0.09	0.08	0.09	0.12	0.09	0.05	0.12	0.14	0.12	0.14	0.15	0.05	0.07	0.07	0.10	0.12	0.12	0.09	0.08
MgO	%	35.7	38.2	37.0	38.3	35.2	37.9	36.5	37.5	34.5	36.3	36.41	34.98	36.0	33.9	36.7	35.4	39.4	39.2	38.5	37.3	38.0	36.0	37.3	37.5
CaO	%	0.15	0.15	0.06	0.06	0.15	0.10	0.18	0.05	0.07	0.39	0.77	0.18	0.10	3.19	0.09	3.23	0.08	0.10	0.09	0.07	0.48	0.43	0.39	0.12
Na_2O	%	<0.01	<0.01	<0.01	<0.01	<0.01	<0.01	<0.01	<0.01	<0.01	<0.01	<0.01	<0.01	<0.01	<0.01	<0.01	<0.01	<0.01	<0.01	<0.01	<0.01	<0.01	<0.01	<0.01	<0.01
K_2O	%	<0.01	<0.01	<0.01	<0.01	<0.01	<0.01	<0.01	<0.01	<0.01	<0.01	<0.01	<0.01	<0.01	<0.01	<0.01	<0.01	<0.01	<0.01	<0.01	<0.01	<0.01	<0.01	<0.01	<0.01
P_2O_5	%	0.01	0.01	0.01	0.01	0.01	0.01	0.01	0.01	0.01	0.02	0.01	0.02	0.01	0.01	0.01	0.01	0.01	0.01	0.01	0.02	0.01	0.01	0.01	0.01
LOI	%	14.4	14.4	12.7	13.8	15.2	14.8	14.0	14.4	11.7	11.8	12.1	10.0	11.2	9.9	12.4	13.9	14.2	10.6	13.3	13.0	13.1	12.9	13.6	12.3
Sum	%	101.8	101.2	100.9	102.6	101.8	102.2	101.7	101.8	101.0	101.6	101.9	100.9	101.0	100.9	101.0	101.1	103.1	99.5	100.6	102.4	101.3	102.1	101.8	101.4
Co	ppm	107	109	112	97	120	110	92	91	99	83	97	92	95	110	89	105	98	102	98	120	110	110	106	108
Cr	ppm	2900	2380	2380	2510	2400	2910	2720	1500	2510	2710	2460	2540	2670	2400	3110	2790	2480	2710	2270	2880	2530	2780	3380	2550
Ni	ppm	2580	2560	1850	2250	3180	2350	2970	2510	2950	1970	2110	1970	2210	2010	2360	2330	2340	2400	2370	2390	2340	2190	2370	2380
V	ppm	62	36	24	31	54	38	33	26	64	67	51	50	46	81	44	51	23	47	27	25	33	30	44	39
Zn	ppm	65	48	42	36	51	46	52	53	58	66	43	55	61	53	61	50	54	41	54	74	59	69	54	65
Pb	ppm	0.04	0.04	0.04	0.07	0.21	0.02	0.02	0.14	0.03	0.47	0.05	0.08	0.19	0.01	0.03	0.31	0.87	1.4	1.4	0.68	0.97	2.9	1.3	1.3
Cu	ppm	15	4.2	62	12	8.4	8.8	2.6	4.4	27	4.8	6.9	4.0	3.4	3.5	n.a.	n.a.	2.9	3.1	1.8	3.3	0.84	0.66	3.9	0.71
S	ppm	20	320	9.3	19	6.7	140.0	8.4	13	2.4	2.3	620	69	<1.0	46	n.a.	n.a.	35	23	4.5	35	23	120	26	28
Os	ppb	2.36	4.29	2.94	3.48	4.43	5.96	6.41	4.09	1.88	2.57	2.96	2.62	3.47	2.45	n.a.	n.a.	6.60	6.18	n.a.	4.07	3.36	6.38	n.a.	n.a.
Ir	ppb	3.45	4.58	3.22	3.75	5.05	3.74	4.87	4.21	3.13	2.23	2.93	2.90	3.60	2.25	n.a.	n.a.	4.05	4.95	n.a.	4.79	3.64	6.19	n.a.	n.a.
Ru	ppb	6.98	7.53	7.56	8.66	8.67	6.89	15.37	6.16	6.17	5.97	5.90	4.22	7.32	4.21	n.a.	n.a.	10.3	11.3	n.a.	8.83	6.06	12.03	n.a.	n.a.
Pt	ppb	6.53	7.37	6.54	10.62	8.67	9.42	6.55	6.83	6.13	4.12	4.42	17.07	2.21	3.91	n.a.	n.a.	4.89	8.99	n.a.	7.05	5.76	11.77	n.a.	n.a.
Pd	ppb	6.17	4.33	4.75	8.19	6.39	6.02	1.79	2.30	1.86	3.22	1.77	10.19	3.38	0.90	n.a.	n.a.	5.63	5.02	n.a.	2.84	3.55	2.73	n.a.	n.a.
Bulk Mg#†		88.3	90.6	88.0	90.3	88.4	89.8	88.7	89.9	88.0	90.2	90.1	89.5	89.4	87.2	86.7	86.8	90.7	91.0	90.2	88.3	89.6	88.6	89.6	89.4

Note: n.a.—not analyzed; SFZ—Septentrional fault zone; LOI—loss on ignition.

*Fe total expressed as Fe_2O_3.

†Bulk Mg# = atomic Mg*100/(Mg + total Fe).

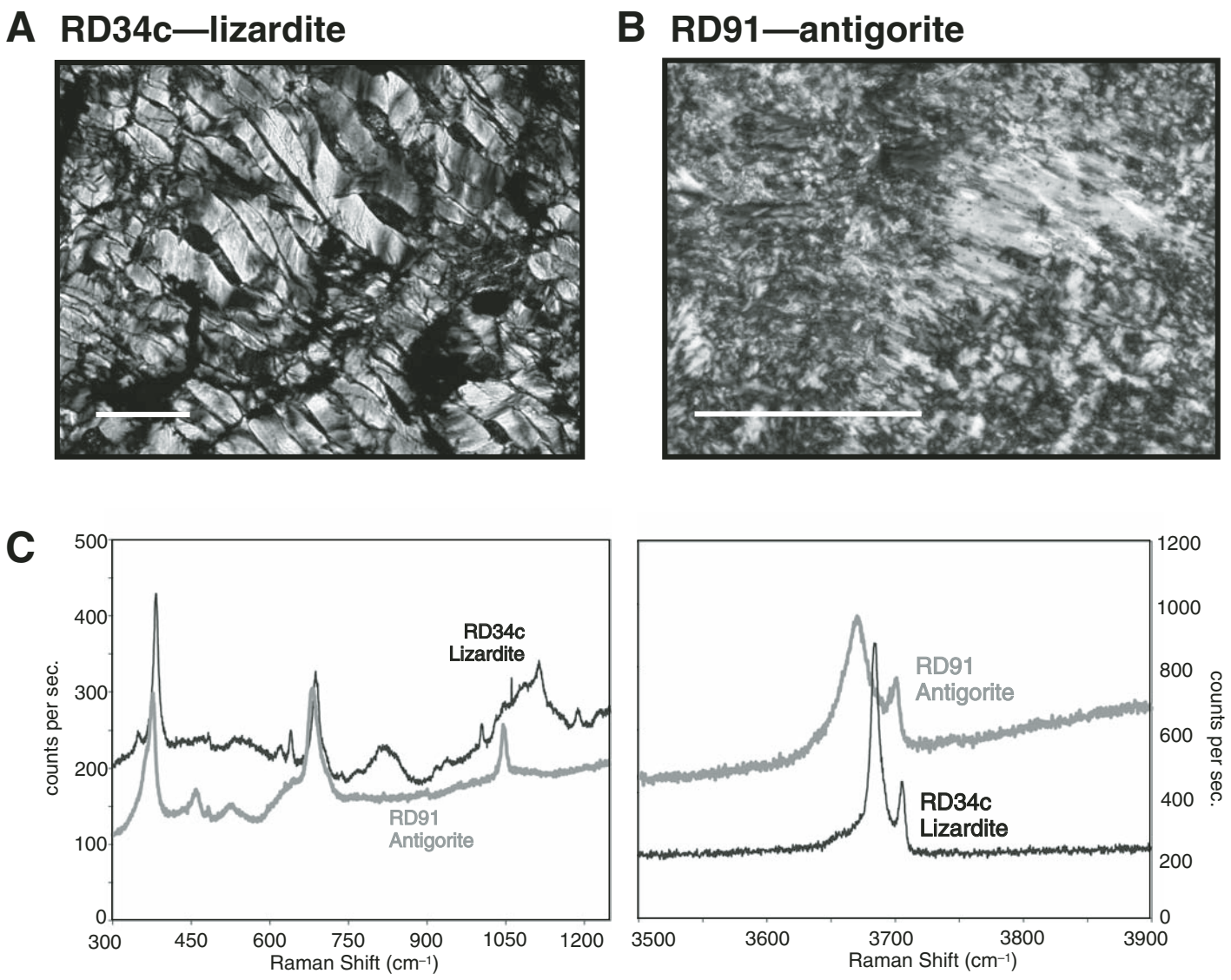

Figure 3. Photomicrographs of serpentinites under crossed polars. Scale bars are 0.3 mm. (A) Foliated flaky lizardite in sample RD34c. (B) Well-crystallized blades of antigorite in an antigorite-rich matrix in sample RD91. (C) Micro-Raman spectra from flaky lizardite (sample RD34c) and large blades of antigorite (sample RD91), for Raman shifts between 300 cm^{-1} and 1200 cm^{-1} (Si-O and Mg-O bonds) and between 3500 cm^{-1} and 3900 cm^{-1} (OH bonds). Spectra of RD34c between 300 cm^{-1} and 1200 cm^{-1} are affected by background radiation. A frequency-doubled Nd-YAG laser (532 nm, 50 mW) was focused to an area of 10 μm in diameter on the surface of a sample. Reference data for Raman spectra of serpentine minerals are from Rinaudo et al. (2003), Auzende et al. (2004), and Groppo et al. (2006).

Cr (>2400 ppm) compared to primitive mantle values (McDonough and Sun, 1995), suggesting that all samples are residual mantle peridotites after partial melting.

Bulk-rock compositions suggest that the protoliths for serpentinite samples from the fault zones are more refractory than those for samples from tectonic mélanges and the northern terranes. Fault-zone serpentinite samples have higher MgO (average 37.5 wt%) and lower Al_2O_3 (<0.75 wt%) than the other two types of serpentinites (average 36.1 wt% MgO and 1.0–3.0 wt% Al_2O_3). Fault-zone serpentinites show a vertical array at low Al/Si, within the field of forearc mantle peridotites in terms of Al/Si versus Mg/Si weight ratios (Hattori and Guillot, 2007; Fig. 7), whereas serpentinite samples from the tectonic mélanges and the northern terranes plot in the field of abyssal peridotites (Fig. 7).

Platinum Group Elements

Iridium-group PGEs (Ir, Os, and Ru) remain in the mantle during partial melting, whereas Pd-group PGEs (Pt, Pd, and Rh) partition to the melt (e.g., Brenan et al., 2005). All samples, with the exception of tectonic mélange sample RD94, have flat to negatively sloped primitive mantle–normalized spectra (Fig. 8). The data confirm that they are all mantle residues. The slightly high contents of Pd-group PGEs in some samples may be due to their mobility in aqueous fluids (Hinchey and Hattori, 2005; Hattori and Cameron, 2004). Tectonic mélange sample RD94 contains exceptionally high Pt and Pd, which may be related to late veinlets of tremolite and chlorite.

Ir-group PGE concentrations for samples from the two fault zones are higher than

primitive mantle values (Fig. 8A). High Ir-group PGE values, along with low Cu, are consistent with the highly refractory nature of these serpentinites. Samples from the northern terranes plot very close to primitive mantle values, suggesting that they are mantle residues that underwent minor degrees of partial melting (Fig. 8B). Samples from the tectonic mélanges show the fractionated PGE patterns, with low contents of Pd-group PGEs (Fig. 8B).

DISCUSSION

Origins of the Serpentinites

The geochemical data of this study indicate that serpentinites from the tectonic mélanges and the northern terranes are hydrated abyssal peridotites, whereas serpentinites along the fault zones were originally forearc mantle peridotites (Fig. 7). High values of Cr# for spinel also support highly refractory protoliths for serpentinites along the strike-slip fault zones, since Cr# of spinel increases with increasing degrees of partial melting (e.g., Dick and Bullen, 1984).

Spinels in fault-zone samples RD6–81 and RD18b have relatively high Cr#, suggesting that the protoliths for these serpentinites may be either refractory abyssal peridotites or relatively fertile forearc mantle peridotites (Fig. 5A). The former possibility, refractory abyssal peridotite origin, is not likely because refractory abyssal peridotites form at fast-spreading ridges, such as the East Pacific Rise (Niu and Hekinan, 1997). Abyssal peridotites formed at slow-spreading ridges commonly contain spinel with low Cr#, i.e., <0.40 (Michael and Bonatti, 1985). The proto-Caribbean lithosphere was produced at the proto–Caribbean Ridge, which had an ultraslow spreading rate between 0.5 and 2 cm/a (Meschede and Frisch, 1998). Therefore, spinel grains in the abyssal peridotites of the proto–Caribbean plate likely contain very low Cr#. These spinel grains observed in our fault-zone serpentinite samples are interpreted to be forearc mantle origin. In addition, the proposed interpretation, a forearc mantle origin for these fault-zone serpentinites, is further supported by high Ir-group PGE contents (Fig. 8) and low Al/Si ratios of their bulk-rock compositions (Fig. 7).

Cr-spinel grains in samples from the northern terranes plot in the abyssal peridotite field (Fig. 5). Among them, spinel from northern terrane samples RD8b and RD31 shows relatively high Cr# (~0.6) and YFe^{3+} (~0.1), and they are interpreted to be abyssal plagioclase peridotites because of relatively high Al_2O_3 (1.6 and 1.44 wt%; Table 2). Plagioclase peridotites constitute ~30 vol% of abyssal peridotites on the seafloor (Dick and Bullen, 1984); however, plagioclase was not identified in our samples.

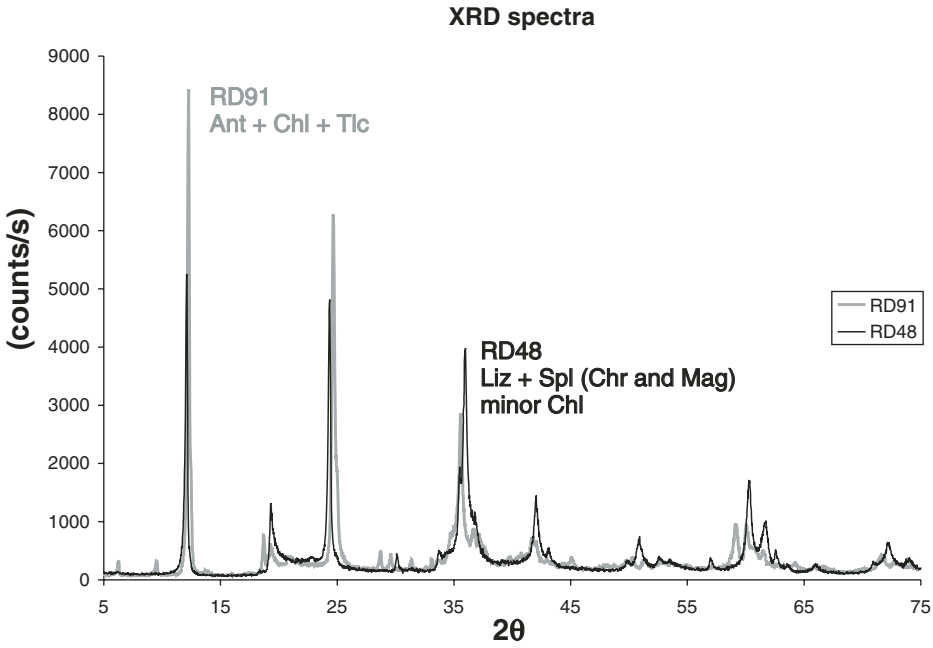

Figure 4. Selected bulk-rock X-ray diffraction (XRD) spectra: lizardite is identified in samples from near fault zones and in the northern terranes (example RD48), whereas antigorite is the major mineral in tectonic mélanges in the central part of the Rio San Juan Complex (example RD91).

Considering the very low Ca and Na in our samples, the original amount of plagioclase was low and was altered during serpentinization.

Serpentinites associated with late strike-slip fault zones in our samples are similar in composition to serpentinites along the Puerto Rico Trench (Bowin et al., 1966) and the Zaza fault zone in Cuba (Hattori and Guillot, 2007) (Fig. 7). Spinel grains in these samples also show similar Cr# (~0.47–0.69 for fault zone samples, ~0.55 for the Puerto Rico Trench and ~0.56 for Cuba). The latter two are also considered to have originated from the forearc mantle wedge (Bowin et al., 1966; Hattori and Guillot, 2007). The similarities in compositions are consistent with their common formation in the same subduction system.

These forearc mantle serpentinites from the northern margin of the Caribbean plate have relatively low Mg/Si ratios in bulk-rock composition (Fig. 7) and moderate Cr# in spinel compared to the Mariana forearc serpentinites (Cr# up to 0.82; Fig. 5; Ishii et al., 1992) and in Ladakh, western Himalayas (Cr# up to 0.84; Guillot et al., 2001). The data suggest that the northern Caribbean mantle wedge was relatively fertile compared to those of other well-documented mature subduction zones. The relatively fertile nature of the forearc peridotites may reflect the short-lived nature of the subduction zone and the small volume of arc igneous rocks produced compared to the two other well-studied sites. Subduction in Hispaniola lasted less than 50 Ma (Pindell et al., 1988), whereas subduction in the western Pacific has been in operation for more than 200 Ma, and subduction in the western Himalayas has been in operation for over 150 Ma. The latter subduction zones have produced large quantities of arc igneous rocks in Japan and the southern margin of Eurasia.

Hydrated Abyssal Peridotites Associated with High-Pressure Rocks

Abundant peridotites were likely exposed to seawater on and near the seafloor of the proto–Caribbean Sea as the oceanic lithosphere formed at a slow-spreading ridge, similar to Atlantic Ocean lithosphere (e.g., Cannat et al., 1995). Serpentinites in the northern terranes and tectonic mélanges originated from abyssal peridotites of the proto-Caribbean lithosphere, and this interpretation is consistent with abundant oceanic metabasites and metagabbros in the area (Pindell and Draper, 1991; Draper and Nagle, 1991).

In the tectonic mélanges, blades of antigorite overprint lizardite, which suggests that the serpentinites underwent metamorphism under blueschist facies conditions (O'Hanley, 1996; Auzende et al., 2002). Antigorite is the predominant serpentine species in high-pressure tectonic mélanges worldwide (e.g., O'Hanley, 1996),

TABLE 3. COMPOSITIONS OF SELECTED CR-SPINEL GRAINS IN SERPENTINITES

Locality:	Northern terranes				Camú fault zone				Septentrional fault zone				
Sample:	RD4	RD6a	RD8b	RD31	RD9a	RD18b	RD6-80	RD6-81	RD45	RD48	RD34c	RD68	RD6-36a
SiO_2 (wt%)	<0.01	0.06	0.07	0.04	0.05	0.04	0.02	0.01	0.01	<0.02	<0.02	<0.02	<0.02
Al_2O_3	50.28	34.91	23.18	24.07	23.07	27.42	15.84	29.62	16.04	19.03	23.24	27.93	20.62
TiO_2	0.07	0.09	0.27	0.01	0.04	0.07	0.06	0.06	0.07	0.21	0.08	0.04	0.11
V_2O_3	n.a.	0.17	0.25	0.25	0.25	0.23	0.25	0.18	0.27	0.22	0.28	0.28	n.a.
Cr_2O_3	18.64	33.22	37.77	43.18	45.69	40.76	52.68	38.39	46.99	44.89	40.31	38.65	42.18
Fe_2O_3*	0.96	2.03	9.15	3.65	1.92	2.32	2.67	3.24	7.05	5.49	5.69	2.25	6.48
FeO*	13.27	14.01	17.77	17.36	17.16	16.14	18.33	15.21	21.45	20.47	19.50	19.07	20.51
MgO	17.34	15.31	11.68	12.04	12.06	13.12	10.59	14.08	8.22	9.01	9.93	10.77	9.09
MnO	0.07	0.07	0.24	0.13	0.08	0.14	0.09	0.09	0.27	0.30	0.28	0.29	0.23
NiO	0.29	0.09	0.1	0.1	0.10	0.06	0.03	0.11	0.04	n.a.	0.10	n.a.	0.12
ZnO	0.27	0.16	0.19	0.24	0.21	0.26	0.22	0.22	0.67	0.80	0.77	0.68	0.53
CaO	0.01	<0.01	<0.01	<0.01	<0.01	0.01	0.01	0.01	0.01	<0.01	0.03	<0.01	0.03
Sum	101.20	100.12	100.67	101.07	100.63	100.57	100.79	101.22	101.09	100.42	100.21	99.97	99.90
O = 32													
Si^{4+}	–	0.013	0.018	0.010	0.013	0.010	0.005	0.003	0.003	0.000	0.000	0.000	0.000
Al^{3+}	12.673	9.496	6.743	6.923	6.681	7.755	4.769	8.218	4.901	5.739	6.859	8.045	6.203
Ti^{4+}	0.011	0.016	0.050	0.002	0.007	0.013	0.012	0.011	0.013	0.039	0.014	0.008	0.021
V^{3+}	n.a.	0.032	0.049	0.048	0.048	0.045	0.050	0.034	0.057	0.044	0.056	0.056	n.a.
Cr^{3+}	3.152	6.063	7.371	8.333	8.876	7.735	10.637	7.146	9.630	9.081	7.981	7.470	8.513
Fe^{3+}	0.154	0.353	1.700	0.670	0.355	0.419	0.513	0.574	1.375	1.057	1.072	0.413	1.245
Fe^{2+}	2.373	2.704	3.667	3.544	3.527	3.240	3.915	2.995	4.651	4.382	4.084	3.899	4.378
Mg^{2+}	5.529	5.266	4.296	4.379	4.416	4.693	4.030	4.940	3.175	3.438	3.706	3.924	3.460
Mn^{2+}	0.013	0.014	0.051	0.028	0.017	0.029	0.018	0.018	0.058	0.066	0.059	0.060	0.051
Ni^{2+}	0.050	0.016	0.021	0.020	0.021	0.011	0.006	0.020	0.009	0.000	0.020	0.000	0.024
Zn^{2+}	0.042	0.027	0.034	0.044	0.038	0.046	0.041	0.038	0.129	0.152	0.142	0.123	0.099
Ca^{2+}	0.002	0.000	0.000	0.000	0.000	0.004	0.003	0.003	0.002	0.001	0.007	0.004	0.007
Sum	24.00	24.00	24.00	24.00	24.00	24.00	24.00	24.00	24.003	23.999	24.000	24.002	24.001
Cr#	0.199	0.390	0.522	0.546	0.571	0.499	0.690	0.465	0.663	0.613	0.538	0.481	0.578
YFe^{3+}	0.010	0.022	0.108	0.042	0.022	0.026	0.032	0.036	0.086	0.067	0.067	0.026	0.078
XMg	0.700	0.661	0.539	0.553	0.556	0.592	0.507	0.623	0.406	0.440	0.476	0.502	0.441

*FeO and Fe_2O_3 contents of spinel were calculated assuming a stoichiometric composition; n.a.—not analyzed. See the definition of Cr#, YFe^{3+} and XMg in the footnote of Table 1.

since it is stable at a wide temperature range up to 700 °C (e.g., Wunder and Schreyer, 1997; Evans, 2004). Furthermore, local amphibolitization in the central Rio San Juan Complex is not only recorded in serpentinites but also in eclogite fragments from the tectonic mélanges (Krebs et al., 2008). This evidence suggests that these serpentinites and the high-pressure fragments in serpentinite mélanges likely have similar thermal histories.

Krebs et al. (2008) suggested that the mélanges represent a serpentinite-rich subduction channel based on pressure-temperature paths of eclogites and blueschists in the mélanges of the Dominican Republic. Our data show that this subduction channel is mostly composed of hydrated abyssal peridotites of the proto-Caribbean lithosphere produced at a slow-spreading ridge. Oceanic plates produced at slow-spreading ridges expose a large part of abyssal peridotites to seawater at and near the seafloor, resulting in the production of abundant serpentinites. Subduction of such an oceanic plate appears to result in a wide serpentinite subduction channel, as has been observed in high-pressure mélanges in the western Alps (Schwartz et al., 2001; Hattori and Guillot, 2007). This is consistent with the numerical model of Gorczyk et al. (2007), which suggests that a wide serpentinite channel will be developed in an oceanic subduction zone where abundant hydrated abyssal peridotites are subducted. The serpentinite channel would incorporate high-pressure rocks from underlying subducting slabs, and fragments of these rocks are then exhumed within the channel, as observed in the mélange units in our study area. This result highlights the importance of hydrated abyssal peridotites in the exhumation of high-pressure rocks in oceanic subduction systems.

The numerical model of Gorczyk et al. (2007) shows that a serpentinite subduction channel may also incorporate overlying hydrated forearc mantle peridotites. It is therefore possible that hydrated forearc mantle serpentinites are included as fragments in the serpentinite mélanges, but the identification and sampling of such serpentinites of forearc mantle origin would be very difficult in the matrix of voluminous serpentinites of abyssal peridotite origin. The two different origins of serpentinites would appear very similar in the field.

In contrast, serpentinites in the northern terranes are dominated by low-temperature lizardite and magnetite, and they contain well-preserved grains of primary Cr-spinel, suggesting that these abyssal peridotites were buried to, at most, lower greenschist conditions.

Hydration of Forearc Peridotites at Shallow Depths

Antigorite is commonly associated with high-pressure rocks exhumed from the mantle (e.g., O'Hanley, 1996; Auzende et al., 2002), but lizardite and chrysotile have been reported as the major constituents of several samples in the Mariana forearc mantle serpentinites (Ohara and Ishii, 1998; D'Antonio and Kristensen, 2004), as they form at depths of 25–30 km (e.g., Fryer et al., 1999) and at temperatures <300 °C (Benton et al., 2001). Hydration of forearc mantle peridotites at shallow depths, <25 km, is also suggested in the western Himalayas, based on the presence of As(V) in forearc mantle serpentinites (Hattori et al., 2005).

In our study area, lizardite is the dominant species of serpentinites along fault zones. Assuming a geothermal gradient of ~8 °C/km in this subduction zone (Zack et al., 2004; Escuder-Viruete and Pérez-Estaún, 2006) and lizardite stability up to 300 °C (O'Hanley 1996; Evans, 2004), the maximum depth is 35 km. Considering that peridotites are hydrated in the forearc at shallow depths far above the subduction plate, these peridotites likely originated from the forearc mantle at depths much shallower than 35 km.

Different Forearc Sources for Septentrional Fault Zone and Camú Fault Zone Serpentinites

Cr-spinels from serpentinites along the Septentrional fault zone have lower XMg values than spinels from the Camú fault zone for a given Cr# (Fig. 5A). Spinel XMg is controlled

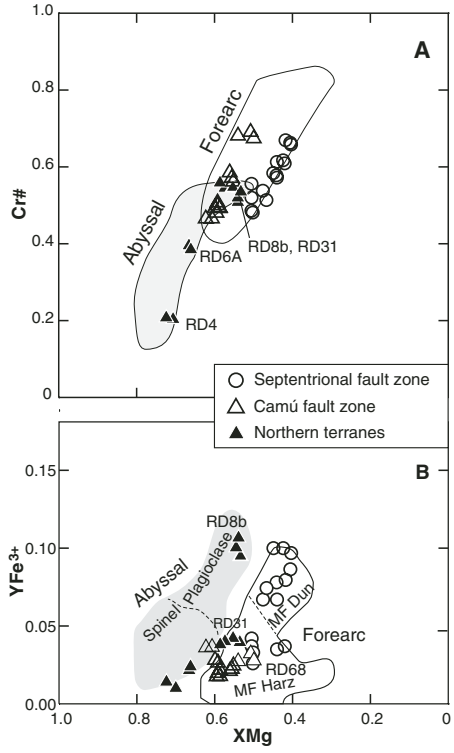

Figure 5. The composition of spinel cores from serpentinites. Each point represents the composition of the core of one grain. The fields of abyssal peridotite include both abyssal spinel peridotite and abyssal plagioclase peridotite (Dick and Bullen, 1984). The forearc mantle peridotite field is defined by Cr-spinel data from serpentinized peridotites exhumed in the Mariana forearc (Ishii et al., 1992). (A) Plot of Cr# versus XMg of Cr-spinels. Samples RD31 and RD8b plot in the field of abyssal plagioclase peridotite (Dick and Bullen, 1984). Note the different trends for Septentrional fault zone and Camú fault zone serpentinites in the forearc mantle peridotite field. (B) Plot of YFe^{3+} versus XMg of Cr-spinels (MF Harz—Mariana forearc harzburgite; MF Dun—Mariana forearc dunite; Ishii et al., 1992). Cr-spinels in serpentinites from the two strike-slip fault zones are similar to those of forearc mantle peridotites.

TABLE 4. COMPOSITIONS OF SELECTED SILICATE MINERALS

	Olivine				Orthopyroxene			
Locality:	Mélange*		SFZ	Locality:	CFZ	SFZ		Mélange*
Sample:	RD6-52a	RD94	RD68	Sample:	RD18B	RD68	RD34a	RD94
SiO_2 (wt%)	40.41	41.45	41.72	SiO_2 (wt%)	57.14	57.22	57.03	57.48
Al_2O_3	<0.02	<0.02	<0.02	Al_2O_3	2.23	1.67	1.45	1.72
MgO	48.06	49.05	51.22	MgO	34.42	34.92	34.34	34.29
FeO	10.64	9.61	9.27	FeO	5.75	5.74	6.87	6.75
CaO	<0.02	0.03	<0.02	CaO	0.79	0.26	0.3	0.2
Cr_2O_3	<0.02	n.a.	0.01	Cr_2O_3	0.66	0.4	0.39	0.08
MnO	0.21	0.11	0.21	MnO	0.15	0.15	0.19	0.14
TiO_2	0.01	n.a.	n.a.	TiO_2	0.02	0.04	0.02	0.08
NiO	0.34	0.5	n.a.	NiO	<0.02	0.04	<0.02	n.a.
				Na_2O	<0.02	0.01	<0.02	<0.01
Sum	99.67	100.75	102.43	Sum	101.16	100.45	100.59	100.75
O = 4				**O = 6**				
Si^{4+}	0.999	1.007	0.995	Si^{4+}	1.947	1.959	1.961	1.967
Al^{3+}	0.000	0.000	0.000	Al^{3+}	0.089	0.051	0.059	0.069
Mg^{2+}	1.771	1.777	1.821	Mg^{2+}	1.748	1.782	1.760	1.749
Fe^{2+}	0.220	0.195	0.185	Fe^{2+}	0.164	0.164	0.198	0.193
Ca^{2+}	0.000	0.001	0.000	Ca^{2+}	0.029	0.011	0.011	0.007
Cr^{3+}	0.000	n.a.	0.000	Cr^{3+}	0.018	0.026	0.010	0.002
Mn^{2+}	0.004	0.002	0.004	Mn^{2+}	0.004	0.004	0.006	0.004
Ti^{4+}	0.000	n.a.	n.a.	Ti^{4+}	0.001	0.001	0.001	0.002
Ni^{2+}	0.007	0.010	n.a.	Ni^{2+}	0.000	0.001	0.000	0.00
Sum	3.001	2.992	3.005	Na^{+}	0.000	0.001	0.000	0.001
Fo	89.0	90.1	90.8	Sum	4.000	4.000	4.006	3.994
				Mg#†	0.914	0.916	0.899	0.901
				En	90.1	91.1	89.4	89.7
				Fs	8.4	8.4	10.1	9.9
				Wo	1.5	0.6	0.6	0.4

Note: n.a.—not analyzed; SFZ—Septentrional fault zone; CFZ—Camú fault zone.
*Mélanges in central Rio San Juan Complex.
†Mg# = atomic ratio of Mg/(Mg + Fe).

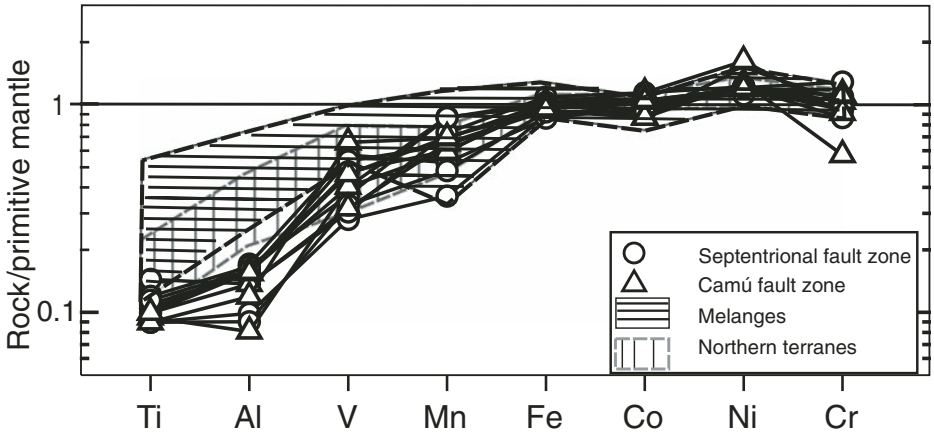

Figure 6. Primitive mantle–normalized immobile elements from serpentinites of the subduction complex in the northern Dominican Republic. All samples are depleted in incompatible elements compared to compatible elements, suggesting that they are mantle residues. Moreover, samples from the Septentrional and Camú fault zones are more depleted in Ti, Al, and V compared to samples from tectonic mélanges and the northern terranes. Primitive mantle values are from McDonough and Sun (1995).

by Mg/(Mg + Fe) in the rocks and temperature. In an environment with similar compositions of olivine, lower XMg values in Cr-spinel are due to lower equilibrium temperatures with olivine at subsolidus conditions (e.g., Evans and Frost, 1975; Wang et al., 2008), caused by cooling of the forearc mantle near the slab interface due to input of slab-derived fluids (Ohara and Ishii, 1998; Okamura et al., 2006). Olivine grains are only preserved in one sample along the Septentrional fault zone and are no longer present in samples along the Camú fault zone, but orthopyroxene is still present in several samples from the two zones, and they have similar Mg# values (Table 1). Assuming that the modal proportions of Cr-spinel are similar in the forearc mantle, we interpret the lower XMg of Septentrional fault zone serpentinites to likely record cooler temperatures than the Camú fault zone before pervasive serpentinization. The proposed interpretation is consistent with higher Fe^{3+} in spinel and higher Pb contents in serpentinites from the Septentrional fault zone than from the Camú fault zone.

Spinel in Septentrional fault zone serpentinites contains higher YFe^{3+} than spinel in the

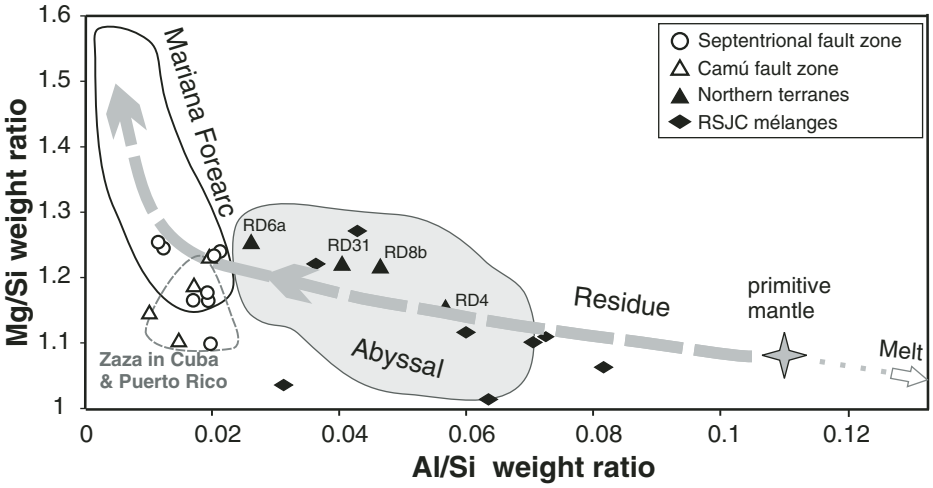

Figure 7. Weight ratios of Mg/Si versus Al/Si of peridotites of various origins (modified from Hattori and Guillot, 2007). The diagram was based on the compositional variation of mantle peridotites compiled by Pearson et al. (2003) and Palme and O'Neill (2003), and abyssal peridotites by Niu (2004). The field of abyssal peridotite is defined by the 7th and 93rd percentile values of the Niu's data. The expected compositional change of residual mantle peridotites during partial melting is shown with a thick gray arrow originating from the primitive mantle values (McDonough and Sun, 1995). Among Mg, Al, and Si, Al is preferentially incorporated into a melt during partial melting, as documented by high Al of magmas compared to peridotites. Therefore, Al contents are lowered in the residue during partial melting, which results in low Al/Si in mantle peridotites. After substantial reduction of Al/Si in the residual mantle peridotites, Mg/Si ratios increase because Si is less compatible with mantle minerals than Mg. This is consistent with higher MgO contents in the depleted mantle composition compared to that of the primitive mantle (Workman and Hart, 2005). These bulk compositional changes, decrease in Al/Si and increase in Mg/Si, correspond to changes in mineralogy and mineral chemistry in the residual mantle peridotites. Aluminum contents decrease and Mg increases in residual phases (e.g., Wang et al., 2008; Arai and Ishimaru, 2008), and the abundance of pyroxenes in residual peridotites decreases during partial melting to form harzburgite and eventually dunite (e.g., Kubo, 2002). The ratio of Mg/Si increases because olivine has higher ratios of Mg/Si than orthopyroxene and because Mg contents of olivine increase in the residue during partial melting. For example, Fo 92 has a Mg/Si ratio of ~1.55 and very low Al/Si, <0.001. Melt has high Al/Si, outside the range of the diagram. For example, Al/Si ratios for normal mid-ocean-ridge (MORB) are greater than 0.38, and Mg/Si ratios are greater than 0.25 (e.g., Workman and Hart, 2005). Therefore, the arrow depicted with "melt" in the lower right of the diagram shows the direction to the compositions of melt. All our samples from the northern Dominican Republic plot as mantle residues, but serpentinites from the two strike-slip faults are highly depleted and plot in the field of forearc mantle peridotites and are similar in composition to the forearc mantle serpentinites along the Zaza fault zone in Cuba (Hattori and Guillot, 2007) and Puerto Rico Trench serpentinites (Bowin et al., 1966). Samples from the tectonic mélanges and the northern terranes (RD6a, RD31, RD4, and RD8b) have compositions similar to abyssal peridotite. Data from the Mariana forearc are from Ishii et al. (1992), Yamamoto et al. (1992), and Parkinson and Pearce (1998). Primitive mantle values were taken from McDonough and Sun (1995).

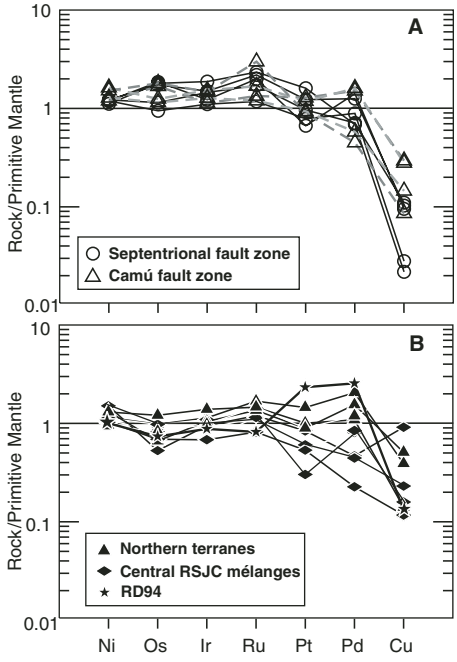

Figure 8. Primitive mantle–normalized values of platinum group elements (PGEs), Ni, and Cu in serpentinites from the northern subduction complex of the Dominican Republic. Elements are placed in order of decreasing compatibility. PGE values for the primitive mantle are 0.00725 times those of carbonaceous chondrites (CI) (McDonough and Sun, 1995): 3.55 ppb Os, 3.30 ppb Ir, 5.18 ppb Ru, 7.32 ppb Pt, and 3.99 ppb Pd. In general, the high content in Ir-group PGEs suggests that serpentinites were initially mantle residues. (A) Data from the two fault zones. (B) Data from the tectonic mélanges and the northern terranes. RSJC—Rio San Juan Complex.

Camú fault zone (Fig. 5B). High YFe^{3+} values reflect high fO_2, suggesting that the peridotites from the Septentrional fault zone probably were exposed to large amounts of slab-derived fluids. Furthermore, Pb is a well-known fluid-mobile element in subduction zones (e.g., Hofmann et al., 1986), it is very soluble in aqueous fluids at low temperatures, <100 °C, and it is enriched in serpentinites at the base of mantle wedges at shallow depths (Hattori and Guillot, 2003, 2007). Serpentinites from the Septentrional fault zone are much higher in Pb (0.68–2.9 ppm) than serpentinites from the Camú fault zone (0.04–0.13 ppm).

These differences in composition can be explained by different locations within the forearc mantle. The protoliths of Septentrional fault zone serpentinites appear to have been relatively closer to the slab compared to those of Camú fault zone serpentinites, which is consistent with both lower temperatures of equilibration and an exposure to larger amounts of slab-derived fluids than the serpentinites along the Camú fault zone.

Protrusion of Forearc Serpentinites along Strike-Slip Fault Zones

The spatial association of mantle-wedge serpentinites with strike-slip fault zones suggests that these serpentinites protruded upward from the base of the forearc mantle along major

fault zones. The Septentrional fault zone and Camú fault zone trend between 090° and 110° and crosscut the original geometry of the NW-trending subduction zone (Mann et al., 1991). The faults cut the once continuous Puerto Plata Complex and Rio San Juan Complex and juxtapose the Pedro Garcia arc terrane against low-grade oceanic rocks of the Puerto Plata Complex (Figs. 2, 9, and 10). More importantly, these oblique fault zones in the study area cut both accretionary and arc terranes, which allowed them to tap hydrated peridotites in the forearc mantle (Fig. 9). In addition, foliation in the Cuaba Gneiss wraps around serpentinite lenses, which suggests that the protrusion of serpentinites occurred during ductile strike-slip faulting of the Cuaba Gneiss.

Serpentinites are common along strike-slip fault zones in many other oceanic subduction zones. Numerous serpentinites are reported along the San Andreas fault (Irwin and Barnes, 1975; Page et al., 1998; Moore and Rymer, 2007) and major strike-slip faults in Guatemala (Harlow et al., 2004). Williams et al. (2006) reported a large ultramafic body that protruded along a major suture zone formed by strike-slip faulting in the Southwest Pacific near New Zealand. We envision a similar scenario for serpentinites along major faults in the northern Dominican Republic, where strike-slip fault zones and serpentinite protrusions were generated in response to syncollisional transpression.

The spatial association of serpentinite bodies along the Septentrional fault zone with garnet peridotites and high-pressure rocks along Rio Cuevas suggests that the protrusion of forearc serpentinites along these fault zones occurred contemporaneous with the late stages of exhumation of metamorphic rocks during collision. Buoyant serpentinites in the fault zone may also have facilitated the exhumation of the high-pressure and ultrahigh-pressure rocks. Goncalves et al. (2000) suggested that conjugate NW-SE extension developed in the northern Dominican Republic under an E-W transtensive condition during the collision of the Caribbean plate with the Bahamas Platform, and that this transtensive condition may have facilitated the exhumation of high-pressure rocks. If so, this local extension regime likely contributed to the protrusion of serpentinites. Serpentinite diapirs in the active Mariana forearc are also interpreted to be primarily located along normal faults developed in an extensional regime (e.g., Fryer et al., 1999).

The mineralogy of the serpentinites in the northern Dominican Republic is very similar to serpentinites found along the San Andreas fault (Page et al., 1998), where strike-slip movement is greatly enhanced by minor talc in the serpentinites (Moore and Rymer, 2007). The strike-slip displacements in the northern Dominican Republic are greater than 60 km along the Camú fault zone (Pindell and Draper, 1991; Draper and Nagle, 1991) and over 200 km along the Septentrional fault zone (Mann et al., 1984; Draper and Nagle, 1991). The movement along strike of the Septentrional fault zone is estimated to be 6–12 mm/a (Prentice et al., 2003). There is seismic activity along the extension of these faults beneath the seafloor, but there is no significant seismic activity along these faults on land (http://neic.usgs.gov/neis/epic). It is therefore possible that talc-bearing forearc mantle serpentinites that protruded along these faults aid the aseismic slip of these large strike-slip faults.

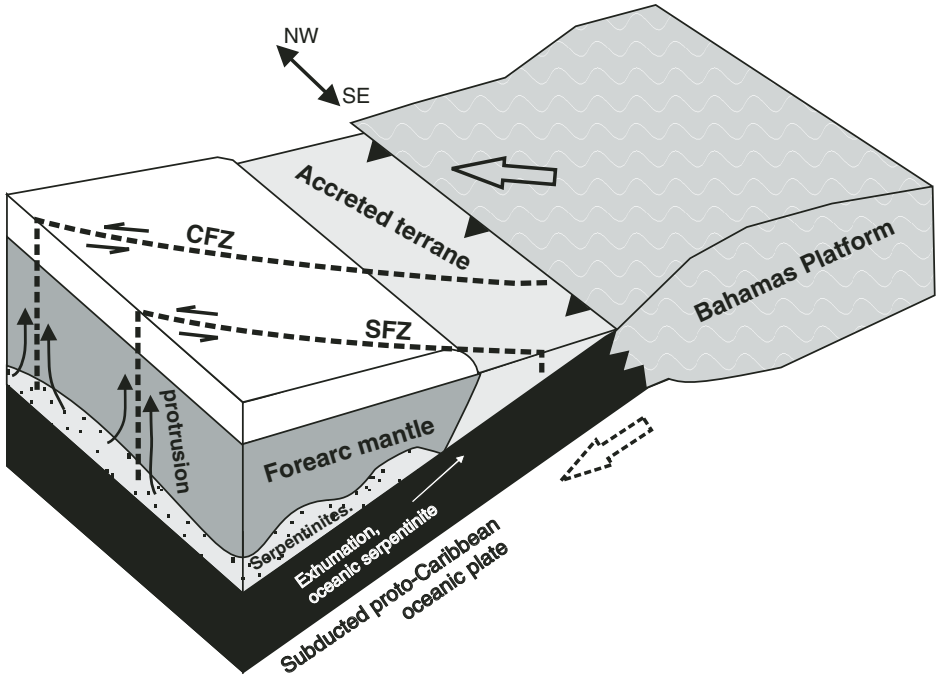

Figure 9. Schematic oblique cross section along the northern Caribbean plate margin in the northern Dominican Republic during the middle Eocene, shortly before the collision with the Bahama Platform, and thus before the development of major strike-slip fault zones. During subduction, hydrated abyssal peridotites formed a serpentinite subduction channel and were exhumed together with blueschists and eclogites (Krebs et al., 2008). Slab-derived fluids hydrated the base of the forearc mantle wedge, forming a layer of serpentinites. The strike-slip fault zones were developed during the collision of the Caribbean plate with the Bahamas Platform, and they obliquely cut the original trend of the subduction complex (Mann et al., 1991). This allowed the fault zones to tap the serpentinized base of the mantle wedge for their protrusion. CFZ—Camú fault zone; SFZ— Septentrional fault zone.

CONCLUSIONS

Two types of serpentinite are recognized in the Tertiary subduction complex of northern Dominican Republic: hydrated abyssal peridotites and forearc mantle wedge peridotites. Abyssal peridotites occur in high-pressure and low-temperature serpentinite tectonic mélanges and low-grade serpentinite terranes. The occurrence of voluminous hydrated abyssal peridotites suggests that they were abundant on and near the seafloor in the subducted proto-Caribbean slab, which is consistent with the formation of the proto-Caribbean oceanic lithosphere at a slow-spreading ridge. Tectonic mélanges containing clasts of high-pressure rocks likely represent a subduction channel developed along the subduction plane of proto-Caribbean oceanic lithosphere and the overlying forearc mantle wedge; our results suggest that oceanic serpentinites contribute to the exhumation of high-pressure rocks.

Hydrated forearc mantle wedge peridotites occur along major strike-slip fault zones that formed during the collision of the Caribbean plate with the Bahamas Platform. Forearc serpentinites were hydrated at the base of the mantle wedge at shallow depths (much less than 35 km). Their association with late strike-slip faults indicates that serpentinites protruded from the mantle wedge to the surface along the

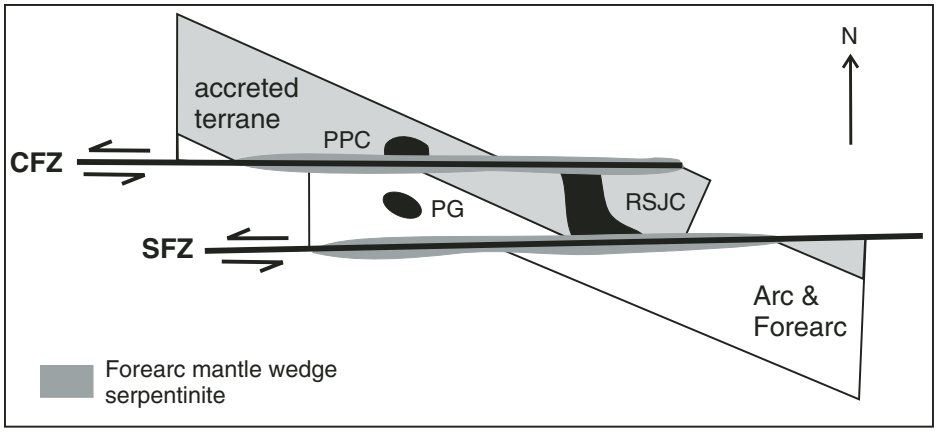

Figure 10. Schematic view of the subduction complex after collision and displacement along the Septentrional fault zone (SFZ) and the Camú fault zone (CFZ). The oblique fault zones cut accretionary and arc terranes and tapped the underlying mantle wedge, allowing the protrusion of ductile and buoyant serpentinites along the strike of the fault zones. The once continuous ophiolitic complex (Draper and Nagle, 1991) was displaced into the Puerto Plata Complex (PPC) and the Rio San Juan Complex (RSJC). PG—Pedro Garcia Complex.

Septentrional fault zone and Camú fault zone. Since serpentinites occur along major faults in many subduction zones, the protrusion of mantle-wedge serpentinites may be a common process at convergent margins, and such rocks may be responsible for aseismic movement along major strike-slip faults.

ACKNOWLEDGMENTS

This paper represents part of the senior author's M.Sc. thesis project at the University of Ottawa. We thank Peter Jones for his assistance with the electron microprobe, Monika Wilk-Alemany for analytical assistance, Ron Hartree for X-ray fluorescence (XRF) and X-ray diffraction (XRD) analyses, George Mrazek for preparation of polished sections, Serge Desgreniers for assistance with Raman spectroscopy, Mahmood Salman for analytical assistance, and Nimal De Silva for help on the ICP-AES. We also thank Olivier Vidal for valuable insights during field work. The project was funded in part by a Discovery Grant from the Natural Science and Engineering Research Council of Canada (NSERC) to Hattori and grants under the DYETI program of Institut National des Sciences de l Univers—Centre National de la Recherche Scientifique to Guillot. Saumur acknowledges financial support of an NSERC Graduate Scholarship, an Ontario Graduate Scholarship, an FQRNT Québec Graduate Scholarship, and a University of Ottawa Excellence Scholarship.

REFERENCES CITED

Abbott, R.N., Jr., Draper, G., and Broman, B.N., 2006, *P-T* path for ultrahigh-pressure garnet ultramafic rocks of the Cuaba Gneiss, Rio San Juan Complex, Dominican Republic: International Geology Review, v. 48, p. 778–790, doi: 10.2747/0020-6814.48.9.778.

Allen, D.E., and Seyfried, W.E., Jr., 2003, Compositional controls on vent fluids from ultramafic-hosted hydrothermal systems at mid-ocean ridges: An experimental study at 400 °C, 500 bars: Geochimica et Cosmochimica Acta, v. 67, p. 1531–1542, doi: 10.1016/S0016-7037(02)01173-0.

Arai, S., and Ishimaru, S., 2008, Insights into petrological characteristics of the lithosphere of mantle wedge beneath arcs through peridotite xenoliths: A review: Journal of Petrology, v. 49, p. 665–695, doi: 10.1093/petrology/egm069.

Auzende, A., DeVouard, B., Guillot, S., Daniel, I., Baronnet, A., and Lardeaux, J., 2002, Serpentinites from Central Cuba: Petrology and HRTEM study: European Journal of Mineralogy, v. 14, p. 905–914, doi: 10.1127/0935-1221/2002/0014-0905.

Auzende, A.L., Daniel, I., Reynard, B., Lemaire, C., and Guyot, F., 2004, High-pressure behaviour of serpentine minerals; a Raman spectroscopic study: Physics and Chemistry of Minerals, v. 31, p. 269–277, doi: 10.1007/s00269-004-0384-0.

Benton, L.D., Ryan, J.G., and Tera, F., 2001, Boron isotope systematics of slab fluids as inferred from a serpentine seamount, Mariana forearc: Earth and Planetary Science Letters, v. 187, p. 273–282, doi: 10.1016/S0012-821X(01)00286-2.

Bowin, C.O., Nalwalk, A.J., and Hersey, J.B., 1966, Serpentinized peridotite from the north wall of the Puerto Rico Trench: Geological Society of America Bulletin, v. 77, p. 257–269, doi: 10.1130/0016-7606(1966)77[257:SPFTNW]2.0.CO;2.

Brenan, J.M., McDonough, W.F., and Ash, R., 2005, An experimental study of the solubility and partitioning of iridium, osmium and gold between olivine and silicate melt: Earth and Planetary Science Letters, v. 237, p. 855–872, doi: 10.1016/j.epsl.2005.06.051.

Calais, E., Perrot, J., and Mercier de Lepinay, B., 1998, Strike-slip tectonics and seismicity along the northern Caribbean plate boundary from Cuba to Hispaniola, Dolan, J.F., and Mann, P., eds., Active strike-slip and collisional tectonics of the northern Caribbean: Geological Society of America Special Paper 326, p. 125–141.

Cannat, M., Mëvel, C., Maia, M., Deplus, C., Durand, C., Gente, P., Agrinier, P., Belarouchi, A., Dubuisson, G., Humler, E., and Reynolds, J., 1995, Thin crust, ultramafic exposures, and rugged faulting patterns at the Mid-Atlantic Ridge (22°–24°N): Geology, v. 23, p. 49–52, doi: 10.1130/0091-7613(1995)023<0049:TCUEAR>2.3.CO;2.

D'Antonio, M., and Kristensen, M.B., 2004, Serpentine and brucite of ultramafic clasts from the South Chamorro Seamount (Ocean Drilling Program Leg 195, Site 1200); inferences for the serpentinization of the Mariana forearc mantle: Mineralogical Magazine, v. 68, p. 887–904, doi: 10.1180/0026461046860229.

Dick, H.J.B., and Bullen, T., 1984, Chromian spinel as a petrogenetic indicator in abyssal and alpine-type peridotites and spatially associated lavas: Contributions to Mineralogy and Petrology, v. 86, p. 54–76, doi: 10.1007/BF00373711.

Dobson, D.P., Meredith, P.G., and Boon, S.A., 2002, Simulation of subduction zone seismicity by dehydration of serpentine: Science, v. 298, p. 1407–1410, doi: 10.1126/science.1075390.

Dolan, J.F., Mullins, H.T., and Wald, D.J., 1998, Active tectonics of the north-central Caribbean; oblique collision, strain partitioning, and opposing subducted slabs, Dolan, J.F., and Mann, P., eds., Active strike-slip and collisional tectonics of the northern Caribbean: Geological Society of America Special Paper 326, p. 1–61.

Draper, G., and Nagle, F., 1991, Geology, structure, and tectonic development of the Rio San Juan Complex, northern Dominican Republic, *in* Mann, P., Draper, G., and Lewis, J.F., eds., Geologic and tectonic development of the North America-Caribbean plate boundary in Hispaniola: Geological Society of America Special Paper 262, p. 77–95.

Dungan, M.A., 1977, Metastability in serpentine-olivine equilibria: The American Mineralogist, v. 62, p. 1018–1029.

Ernst, W.G., ed., 2004, Serpentine and Serpentinites: Mineralogy, Petrology, Geochemistry, Ecology, Geophysics, and Tectonics—A Tribute to Robert G. Coleman: Geological Society of America Special Paper, 616 p.

Escuder-Viruete, J., and Pérez-Estaún, A., 2006, Subduction-related *P-T* path for eclogites and garnet glaucophanites from the Samaná Peninsula Basement Complex: International Journal of Earth Sciences, v. 95, p. 995–1017, doi: 10.1007/s00531-006-0079-5.

Evans, B.W., 1977, Metamorphism of Alpine peridotite and serpentinite: Annual Review of Earth and Planetary Sciences, v. 5, p. 397–447, doi: 10.1146/annurev.ea.05.050177.002145.

Evans, B.W., 2004, The serpentinite multisystem revisited; chrysotile is metastable: International Geology Review, v. 46, p. 479–506, doi: 10.2747/0020-6814.46.6.479.

Evans, B.W., and Frost, B.R., 1975, Chrome-spinel in progressive metamorphism; a preliminary analysis: Geochimica et Cosmochimica Acta, v. 39, p. 959–972, doi: 10.1016/0016-7037(75)90041-1.

Fryer, P., Wheat, C.G., and Mottl, M.J., 1999, Mariana blueschist mud volcanism: Implications for conditions within the subduction zone: Geology, v. 27, p. 103–106, doi: 10.1130/0091-7613(1999)027<0103:MBMVIF>2.3.CO;2.

Goncalves, P., Guillot, S., Lardeaux, J.-M., Nicollet, C., and de Lepinay, B.M., 2000, Thrusting and sinistral wrenching in a pre-Eocene HP-LT Caribbean accretionary wedge (Samaná Peninsula, Dominican Republic): Geodinamica Acta, v. 13, p. 119–132, doi: 10.1016/S0985-3111(00)00116-9.

Gorczyk, W., Guillot S., Gerya, T.V., and Hattori, K.H., 2007, Asthenospheric upwelling, oceanic slab retreat and exhumation of UHP mantle rocks: Insights from Greater Antilles: Geophysical Research Letters, v. 34, L21309, doi: 10.1029/2007GL031059.

Groppo, C., Rinaudo, C., Cairo, S., Gastaldi, D., and Compagnoni, R., 2006, Micro-Raman spectroscopy for a quick and reliable identification of serpentine minerals from ultramafics: European Journal of Mineralogy, v. 18, p. 319–329, doi: 10.1127/0935-1221/2006/0018-0319.

Guillot, S., Hattori, K.H., and de Sigoyer, J., 2000, Mantle wedge serpentinization and exhumation of eclogites: Insights from eastern Ladakh, Northwest Himalaya: Geology, v. 28, p. 199–202, doi: 10.1130/0091-7613(2000)28<199:MWSAEO>2.0.CO;2.

Guillot, S., Hattori, K.H., de Sigoyer, J., Naegler, T., and Auzende, A.L., 2001, Evidence of hydration of the mantle wedge and its role in the exhumation of eclogites: Earth and Planetary Science Letters, v. 193, p. 115–127, doi: 10.1016/S0012-821X(01)00490-3.

Harlow, G.E., Hemming, S.R., Ave Lallemant, H.G., Sisson, V.B., and Sorensen, S.S., 2004, Two high-pressure–low-temperature serpentinite-matrix mélange belts, Motagua fault zone, Guatemala: A record of Aptian

and Maastrichtian collisions: Geology, v. 32, p. 17–20, doi: 10.1130/G19990.1.

Hattori, K.H., and Cameron, E.M., 2004, Utilizing the high mobility of palladium in exploration for platinum group element mineralization: Evidence from the Lac des Iles area, Canada: Economic Geology and the Bulletin of the Society of Economic Geologists, v. 99, p. 157–171.

Hattori, K.H., and Guillot, S., 2003, Volcanic fronts form as a consequence of serpentinite dehydration in the forearc mantle wedge: Geology, v. 31, p. 525–528, doi: 10.1130/0091-7613(2003)031<0525:VFFAAC>2.0.CO;2.

Hattori, K.H., and Guillot, S., 2007, Geochemical character of serpentinites associated with high- to ultrahigh-pressure metamorphic rocks in the Alps, Cuba, and the Himalayas: Recycling of elements in subduction zones: Geochemistry, Geophysics, Geosystems, v. 8, p. Q09010, doi: 10.1029/2007GC001594.

Hattori, K.H., Takahashi, Y., Guillot, S., and Johanson, B., 2005, Occurrence of arsenic (V) in fore-arc mantle serpentinites: X-ray absorption spectroscopy study: Geochimica et Cosmochimica Acta, v. 69, p. 5585–5596, doi: 10.1016/j.gca.2005.07.009.

Hinchey, J.G., and Hattori, K.H., 2005, Magmatic mineralization and hydrothermal enrichment of the high grade zone at the Lac des Iles palladium mine, northern Ontario, Canada: Mineralium Deposita, v. 40, p. 13–23, doi: 10.1007/s00126-005-0472-1.

Hofmann, A.W., Jochum, K.P., Seufert, M., and White, W.M., 1986, Nb and Pb in oceanic basalts; new constraints on mantle evolution: Earth and Planetary Science Letters, v. 79, p. 33–45, doi: 10.1016/0012-821X(86)90038-5.

Irwin, W.P., and Barnes, I., 1975, Effect of geologic structure and metamorphic fluids on seismic behavior of the San Andreas fault system in central and northern California: Geology, v. 3, p. 713–716, doi: 10.1130/0091-7613(1975)3<713:EOGSAM>2.0.CO;2.

Ishii, T., Robinson, P.T., and Maekawa, H., Fiske, 1992, Petrological studies of peridotites from diapiric serpentinite seamounts in the Izu-Ogasawara-Mariana forearc, Leg 125, *in* Fryer, P., Pearce, J.A., Stokking, L.B., et al., eds., Proceedings of the Ocean Drilling Program, Scientific Results, Volume 125: College Station, Texas, Ocean Drilling Program, p. 445–485.

Krebs, M., Maresch, W.V., Schertl, H.P., Münker, C., Baumann, A., Draper, G., Idleman, B., and Trapp, E., 2008, The dynamics of intra-oceanic subduction zones: A direct comparison between fossil petrological evidence (Rio San Juan Complex, Dominican Republic): Lithos, v. 103, p. 106–137, doi: 10.1016/j.lithos.2007.09.003.

Kubo, K., 2002, Dunite formation processes in highly depleted peridotite: Case study of the Iwanaidake peridotite, Hokkaido, Japan: Journal of Petrology, v. 43, p. 423–448, doi: 10.1093/petrology/43.3.423.

Lewis, J.F., Draper, G., Bourdon, C., Bowin, C., Mattson, P.O., Maurrasse, F., Nagle, F., and Pardo, G., 1990, Geology and tectonic evolution of the northern Caribbean margin, *in* Dengo, G., and Case, J.E., ed., The Caribbean Region: Boulder, Colorado, Geological Society of America, The Geology of North America, v. H, p. 77–140.

Lewis, J.F., Draper, G., Proenza, J.A., Espaillat, J., and Jiménez, J., 2006, Ophiolite-related ultramafic rocks (serpentinites) in the Caribbean region: A review of their occurrence, composition, origin, emplacement and Ni-laterite soil formation: Geologica Acta, v. 4, p. 237–263.

Lockwood, J.P., 1971, Sedimentary and gravity-slide emplacement of serpentinite: Geological Society of America Bulletin, v. 82, p. 919–936, doi: 10.1130/0016-7606(1971)82[919:SAGEOS]2.0.CO;2.

Mann, P., Burke, K.C., and Matumoto, T., 1984, Neotectonics of Hispaniola; plate motion, sedimentation, and seismicity at a restraining bend: Earth and Planetary Science Letters, v. 70, p. 311–324, doi: 10.1016/0012-821X(84)90016-5.

Mann, P., Draper, G., and Lewis, J.F., 1991, An overview of the geologic and tectonic development of Hispaniola, *in* Mann, P., Draper, G., and Lewis, J.F., eds., Geological and tectonic development of the North American-Caribbean plate boundary zone in Hispaniola: Geological Society of America Special Paper 262, p. 1–28.

McDonough, W.F., and Sun, S.S., 1995, The composition of the Earth: Chemical Geology, v. 120, p. 223–253, doi: 10.1016/0009-2541(94)00140-4.

Meschede, M., and Frisch, W., 1998, A plate-tectonic model for the Mesozoic and early Cenozoic history of the Caribbean plate: Tectonophysics, v. 296, p. 269–291, doi: 10.1016/S0040-1951(98)00157-7.

Michael, P.J., and Bonatti, E., 1985, Peridotite composition from the North Atlantic; regional and tectonic variations and implications for partial melting: Earth and Planetary Science Letters, v. 73, p. 91–104, doi: 10.1016/0012-821X(85)90037-8.

Moore, D.E., and Rymer, M.J., 2007, Talc-bearing serpentinite and the creeping section of the San Andreas fault: Nature, v. 448, p. 795–797, doi: 10.1038/nature06064.

Nagle, F., 1966, Geology of the Puerto Plata area, Dominican Republic [Unpublished Ph.D. thesis]: Princeton, New Jersey, Princeton University, 171 p.

Niu, Y., 2004, Bulk-rock major and trace element compositions of abyssal peridotites: Implications for mantle melting, melt extraction and post-melting processes beneath mid-ocean ridges: Journal of Petrology, v. 45, p. 2423–2458, doi: 10.1093/petrology/egh068.

Niu, Y., and Hekinian, R., 1997, Spreading-rate dependence of the extent of mantle melting beneath ocean ridges: Nature, v. 385, p. 326–329, doi: 10.1038/385326a0.

O'Hanley, D.S., 1996, Serpentinites: Oxford Monographs on Geology and Geophysics 34, 277 p.

Ohara, Y., and Ishii, T., 1998, Peridotites from the southern Mariana forearc: Heterogeneous fluid supply in the mantle wedge: The Island Arc, v. 7, p. 541–558.

Okamura, H., Arai, S., and Kim, Y.U., 2006, Petrology of fore-arc peridotite from the Hahajima Seamount, the Izu-Bonin Arc, with special reference to chemical characteristics of chromian spinel: Mineralogical Magazine, v. 70, p. 15–26, doi: 10.1180/0026461067010310.

Page, B.M., Thompson, G.A., and Coleman, R.G., 1998, Late Cenozoic tectonics of the central and southern Coast Ranges of California: Geological Society of America Bulletin, v. 110, p. 846–876, doi: 10.1130/0016-7606(1998)110<0846:OLCTOT>2.3.CO;2.

Palme, H., and O'Neill, H.St.C., 2003, Cosmochemical estimates of mantle composition, *in* Carlson, R.W., ed., The mantle and core: Treatise on Geochemistry, v. 2, p. 1–28.

Parkinson, I.J., and Pearce, J.A., 1998, Peridotites from the Izu-Bonin-Mariana forearc (ODP Leg 125); evidence for mantle melting and melt-mantle interaction in a suprasubduction zone setting: Journal of Petrology, v. 39, p. 1577–1618, doi: 10.1093/petrology/39.9.1577.

Pearson, D.G., Canil, D., and Shirey, S.B., 2003, Mantle samples included in volcanic rocks: Xenoliths and diamonds, *in* Carlson, R.W., ed., The Mantle and core: Treatise on Geochemistry, v. 2, p. 171–275.

Pindell, J.L., and Draper, G., 1991, Stratigraphy and geological history of the Puerto Plata area, northern Dominican Republic, *in* Geological and tectonic development of the North American-Caribbean plate boundary zone in Hispaniola: Geological Society of America Special Paper 262, p. 97–114.

Pindell, J.L., Cande, S.C., Pitman, W.C., III, Rowley, D.B., Dewey, J.F., LaBrecque, J.L., and Haxby, W.F., 1988, A plate-kinematic framework for models of Caribbean evolution: Tectonophysics, v. 155, p. 121–138.

Pindell, J.L., Kennan, L., Maresch, W.V., Stanek, K.P., Draper, G., and Higgs, R., 2005, Plate-kinematics and crustal dynamics of circum-Caribbean arc-continent interactions: Tectonic controls on basin development in proto-Caribbean margins, *in* Avé Lallemant, H.G., and Sisson, V.B., eds., Caribbean–South American Plate Interactions, Venezuela: Geological Society of America Special Paper 394, p. 7–52.

Prentice, C.S., Mann, P., Pena, L.R., and Burr, G., 2003, Slip rate and earthquake recurrence along the central Septentrional fault, North American–Caribbean plate boundary, Dominican Republic: Journal of Geophysical Research, v. 108, no. B3, 2149, doi: 10.1029/2001JB000442.

Rinaudo, C., Gastaldi, D., and Belluso, E., 2003, Characterization of chrysotile, antigorite and lizardite by FT-Raman spectroscopy: Canadian Mineralogist, v. 41, p. 883–890, doi: 10.2113/gscanmin.41.4.883.

Schwartz, S., Allemand, P.S., and Guillot, S., 2001, Numerical model of effect of serpentinites on the exhumation of eclogitic rocks: Insights from the Monviso ophiolitic massif (western Alps): Tectonophysics, v. 342, p. 193–206.

Wang, J., Hattori, K.H., Li, J.-P., and Stern, C., 2008, Oxidation state of Paleozoic subcontinental lithospheric mantle below the Pali Aike: Lithos, v. 105, p. 98–110, doi: 10.1016/j.lithos.2008.02.009.

Williams, H.A., Cassidy, J., Locke, C.A., and Spörli, K.B., 2006, Delineation of a large ultramafic massif embedded within a major SW Pacific suture using gravity methods: Tectonophysics, v. 424, p. 119–133, doi: 10.1016/j.tecto.2006.07.009.

Workman, R.K., and Hart, S.R., 2005, Major and trace element composition of the depleted MORB mantle (DMM): Earth and Planetary Science Letters, v. 231, p. 53–72, doi: 10.1016/j.epsl.2004.12.005.

Wunder, B., and Schreyer, W., 1997, Antigorite; high-pressure stability in the system MgO-SiO_2-H_2O (MSH): Lithos, v. 41, p. 213–227, doi: 10.1016/S0024-4937(97)82013-0.

Yamamoto, K., Masutani, Y., Nakamura, N., Ishii, T., Tanaka, T., and Togashi, S., 1992, REE characteristics of mafic rocks from a fore-arc seamount in the Izu-Ogasawara region, western Pacific: Geochemical Journal, v. 26, p. 411–423.

Zack, T., Rivers, T., Brumm, R., and Kronz, A., 2004, Cold subduction of oceanic crust: Implications from a lawsonite eclogite from the Dominican Republic: European Journal of Mineralogy, v. 16, p. 909–916, doi: 10.1127/0935-1221/2004/0016-0909.

Manuscript Received 3 September 2008
Revised Manuscript Received 14 January 2009
Manuscript Accepted 15 January 2009

Printed in the USA